JOURNAL OF Applied Polymer SCIENCE

Significant enhancement of fracture toughness and mechanical properties of epoxy resin using CTBN-grafted epoxidized linseed oil

Quang-Vu Bach,[1]* Cuong Manh Vu,[2,3] Huong Thi Vu,[4] Hoa Binh Vu,[5] Tuyen Van Nguyen,[6] Soon Wong Chang,[7] Dinh Duc Nguyen,[7] Tuyet Anh Dang Thi,[6] Vu Ngoc Doan[3]

[1]Sustainable Management of Natural Resources and Environment Research Group, Faculty of Environment and Labour Safety, Ton Duc Thang University, Ho Chi Minh City, Vietnam

[2]Center for Advanced Chemistry, Institute of Research and Development, Duy Tan University, Da Nang, Vietnam

[3]Faculty of Chemical-Physical Engineering, Le Qui Don Technical University, 236 Hoang Quoc Viet, Ha Noi, Vietnam

[4]AQP Research and Control Pharmaceuticals Joint Stock Company (AQP Pharma J.S.C) Dong Da, Ha Noi, Vietnam

[5]Ghent University, Krijgslaan 281 (S4), Ghent, Belgium

[6]Institute of Chemistry, Vietnam Academy of Science and Technology, 18-Hoang Quoc Viet, Cau Giay, Hanoi, Vietnam

[7]Department of Environmental Energy and Engineering, Kyonggi University, Suwon 442-760, Korea

Correspondence to: C. M. Vu (E-mail: vumanhcuong@duytan.edu.vn or E-mail: vumanhcuong309@gmail.com)

ABSTRACT: Carboxyl-terminated poly(acrylonitrile-*co*-butadiene) (CTBN)-grafted epoxidized linseed oil (ELO) (CTBN-*g*-ELO) was synthesized and used as an effective toughener to simultaneously enhance the mechanical properties and fracture toughness of epoxy resin (EP). The ELO was fabricated from linseed oil via epoxidation processing. The characteristics of the ELO and CTBN-*g*-ELO, such as the average molecular weight and chemical structure, were determined using gel permeation chromatography, proton nuclear magnetic resonance, and Fourier transform infrared spectroscopy. The effects of the CTBN-*g*-ELO loading on the characteristics of the EP were investigated in detail. The test results indicated that by adding 15 phr CTBN-*g*-ELO, the tensile strength, impact strength, and critical stress intensity factor (K_{IC}) were significantly increased, by approximately 23.62, 91.8, and 33.8%, respectively, compared with pristine EP. The glass-transition temperature (T_g) and storage modulus, which were examined via dynamic mechanical thermal analysis and differential scanning calorimetry, respectively, exhibited decreasing trends. Scanning electron microscopy revealed that the CTBN-*g*-ELO existed as spherical particles in the EP, helping to stop the crack growth and change the crack growth directions. © 2019 Wiley Periodicals, Inc. J. Appl. Polym. Sci. **2019**, *136*, 48276.

KEYWORDS: critical stress intensity factor; CTBN-grafted ELO; DSC; DMTA; epoxidized linseed oil; epoxy resin; mechanical properties; rheological testing

Received 24 January 2019; accepted 24 June 2019

DOI: 10.1002/app.48276

INTRODUCTION

Polymeric composites are widely applied in various industrial and engineering applications because of their advantages, for example, their high mechanical strength, impact resistance, chemical resistance, fracture toughness, and thermal stability.[1–4] Polymeric matrices used for composite preparation can be classified into two types: thermoplastic and thermoset. Among these, epoxy resin (EP) has become one of the most widely used matrices for fabrication of fiber-reinforced polymer-based composites because of its processability, good mechanical performance, chemical resistance, and compatibility with most fibers.[5–7] However, cured EP has a high sensitivity to external forces, due to its high crosslinking density.[8,9] This disadvantage limits its application in high-technology fields. Many techniques have been successfully employed to enhance the fracture toughness of EP.[10–21]

Interest in finding and using natural source-based reinforcement materials is increasing because of requirements for developing eco-friendly materials and reducing the exhaust due to petroleum-based materials. Many types of eco-friendly additives have been successfully used for developing bio-based composites, such as microfibrillated cellulose,[22] bacterial cellulose,[23,24] silk fibroin,[25] and epoxidized natural rubber.[26] Vegetable oil and its derivatives are among the most natural additives for biocomposite preparation. Many studies have focused on the development of blends of epoxidized vegetable oil and EP.[27–33] Carboxyl-terminated poly(acrylonitrile-*co*-butadiene) (CTBN) is also an effective toughener for epoxy.[34–36] However, no studies on the effects of CTBN-grafted epoxidized linseed oil (CTBN-*g*-ELO) on properties of cured EP have been reported. Separately, the use of CTBN and epoxidized vegetable oil have improved the K_{IC} and

*E-mail: bachquangvu@tdtu.edu.vn

reduced the tensile strength.[29,34] The effects of ELO on properties of EP were investigated in detail by Yim *et al.*[37] Their experimental results indicated that crosslinking density of EP decreased with incorporation of ELO. However, this enhanced the impact strength of the EP. Additionally, the T_g of EP, which was examined via dynamic mechanical thermal analysis (DMTA), decreased with increasing ELO content. Wang *et al.*[34] reported that increasing CTBN loading in EP reduced the tensile strength and elastic modulus because of low modulus of the CTBN embedded in the EP. Conversely, the CTBN improved the elongation at break. The K_{IC} and G_{IC} values were also improved with addition of CTBN and reached their maximum values at 15 phr CTBN. The K_{IC} and G_{IC} values of CTBN/EP specimens increased by 77.6 and 296.8%, respectively, compared with pristine EP. The experiment also revealed a reduction in the T_g of EP with incorporation of CTBN.

We believe that CTBN-*g*-ELO with a large molecular weight can improve both fracture toughness and mechanical properties of an EP. CTBN-*g*-ELO contains CN, OH, COOH, and oxirane groups; thus, it has the advantages of both CTBN and ELO. The nitrile group (CN) with an unshared electron pair in N atom helps to bind the chains together. Both the OH and COOH can participate in the opening reaction of the oxirane group. The oxirane groups in CTBN-*g*-ELO can also be opened by using a hardener. The ELO was synthesized from linseed oil (LO) via epoxidation processing by using an $HCOOH/H_2O_2$ mixture. The chemical structures of the ELO and CTBN-*g*-ELO were confirmed via Fourier transform infrared (FTIR) spectroscopy and proton nuclear magnetic resonance (^{1}H NMR). Scanning electron microscopy (SEM) was performed to evaluate the fracture propagation and fracture behavior of the composites.

EXPERIMENTAL

Materials

The EP bisphenol A (DER-331, viscosity = 13,000 MPa s^{-1}, specific gravity = 1.16, epoxy content = 22.9%) was supplied by Dow Chemicals (Ho Chi Minh City, Vietnam). Diethylenetriamine (specific gravity = 0.949), triphenylphosphine (TPP), molecular weight (M_W = 262.92 g mol^{-1}, purity = 99%), LO, and CTBN ($\bar{M}_W$ = 3600 g mol^{-1}) were supplied by Sigma-Aldrich (Ho Chi Minh City, Vietnamese branch). An H_2O_2 solution (30%) and formic acid (98%) were supplied by Xilong Scientific Co., Ltd. (Xilong, China).

Fabrication of CTBN-Grafted Epoxidized Soybean Oil

First, the ELO was fabricated from LO via epoxidation processing using a two-necked flask. Both LO and formic acid were simultaneously added into the two-necked round flask, which was equipped with a magnetic stirrer and a condenser. This mixture was homogeneously stirred with a speed of 1000 rpm at 50 °C for 20 min. A calculated amount of hydrogen peroxide was slowly dropped into the reaction mixture for 1 h.[26] This reaction mixture was kept under these conditions for another 5 h, followed by cooling to room temperature. This mixture was then washed with distilled water several times to remove excess acid. The water was removed from product by using anhydrous sodium sulfate, and the product was placed in an oven at 65 °C for 12 h.

To synthesize CTBN-*g*-ELO, 0.1 mol of ELO was dissolved in a dimethylformamide (DMF) solvent for 30 min by using a magnetic stirrer. In another beaker, 0.1 mol of CTBN was well dissolved in 20 mL of the DMF solvent, followed by the addition of an ELO solution with magnetic stirring. Thereafter, 2 mg of TPP was introduced to this mixture, with stirring at 125 °C for 36 h. The CTBN-*g*-ELO elastomer was obtained by removing all the DMF solvent using a rotary evaporator. Details regarding synthesis process for CTBN-*g*-ELO are presented in Figure 1.

CTBN-*g*-ELO-Filled Epoxy-Based Composite

Homogeneous mixtures of CTBN-*g*-ELO with different contents ranging from 5 to 20 phr in the EP were obtained using a magnetic stirrer at 60 °C for 1 h. These mixtures were cooled naturally to room temperature. Then, a curing agent (10 wt %) was added for approximately 20 min, followed by degassing using a vacuum pump. Subsequently, these mixtures were quickly introduced into a steel mold, which was coated with a release agent. The curing reaction was conducted at room temperature for 1 day and then at 80 °C for 3 h. The samples were removed from the mold and stored at room temperature for 1 week prior to testing.[14]

FTIR Test

FTIR spectroscopy was performed to verify the success of the grafting process and epoxidation processing (FTIR spectrometer; PerkinElmer Spectrum Two, California, USA). The scanning range was 4000–400 cm^{-1}, and the signal was averaged over 32 scans, at a resolution of 0.1 cm^{-1}, in the transmission mode.

^{1}H NMR Analysis

The ^{1}H NMR spectra of LO, ELO, and CTBN-*g*-ELO were measured using a DRX-400 (Bruker, Ettlingen, Germany) 400-MHz NMR spectrometer with CDCl3 as a solvent.

Average Molecular Weight (Gel Permeation Chromatography)

The average molecular weight of ELO, CTBN-*g*-ELO, EP, and EP/15 CTBN-*g*-ELO were determined using a gel permeation chromatography (GPC) machine (Waters 2690). A tetrahydrofuran solvent was used as a mobile phase, with a flow rate of 1 mL min^{-1} at 40 °C.

Grafting Degree

The grafting degree was calculated using a titration method according to epoxide group content.

$$G_D = \frac{A_{ELO} - A_{(CTBN-g-ELO)}}{A_{ELO}} \times 100\% \quad (1)$$

Here, A_{ELO} and $A_{CTBN\text{-}g\text{-}ELO}$ represent the oxirane contents of ELO and CTBN-*g*-ELO, respectively.

Rheological Testing

The rheological properties of uncured samples were determined using a modular rheometer (MCR102; Anton Paar, Singapore) in the steady-state mode. The test was performed at room temperature (25 °C) with a shear rate in the range of 0–800 s^{-1}.

Differential Scanning Calorimetry

The T_g values of cured resin were examined using differential scanning calorimetry (DSC; NETZSCH Instruments DSC-204). Approximately, 7.7–8.6 mg of cured resin was cut from a cured resin bar and then placed and sealed in an aluminum pan. The

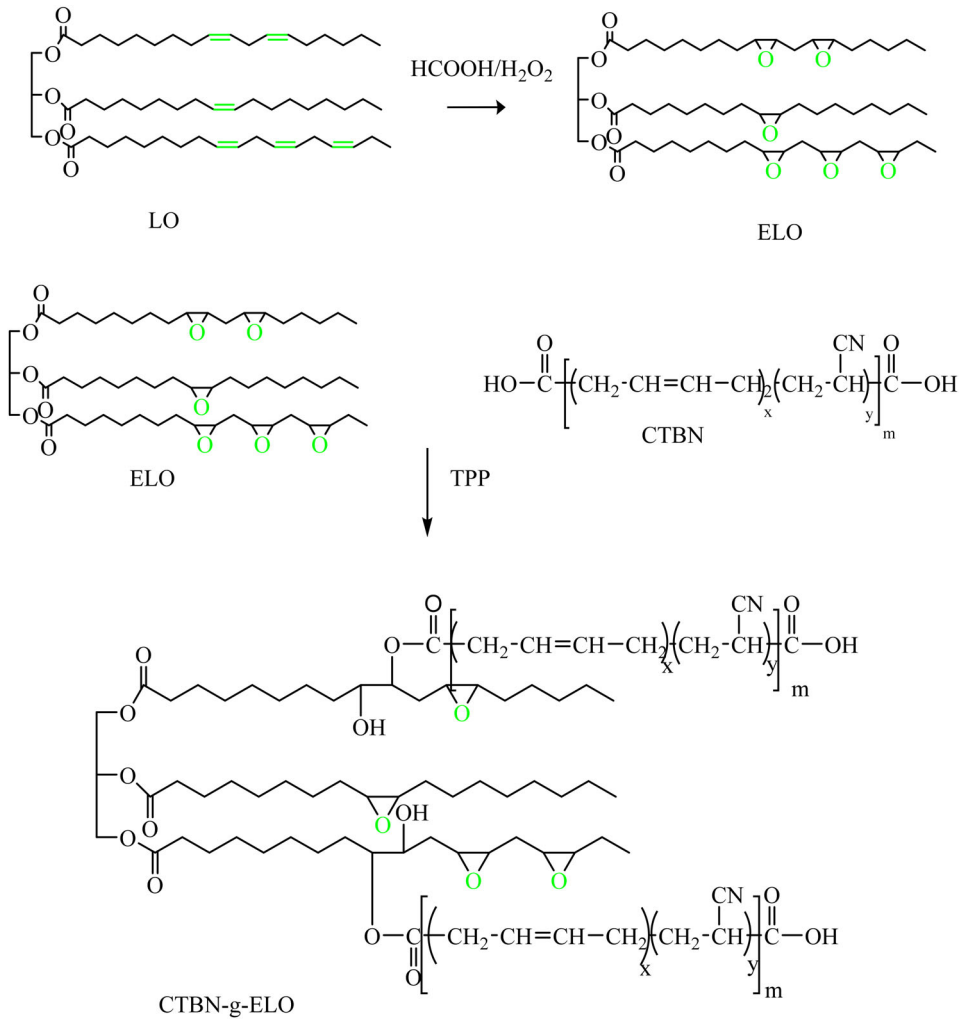

Figure 1. Synthesis of ELO and CTBN-*g*-ELO from LO and CTBN. [Color figure can be viewed at wileyonlinelibrary.com]

samples were heated from 30 to 200 °C at a heating rate of 10 °C min^{-1}.

Thermal Analysis

The thermal characteristics of cured samples were determined using thermogravimetric analysis (TGA; PerkinElmer TGA 4000 System). These samples were heated from 30 to 700 °C in an air atmosphere at a heating rate of 10 °C min^{-1}.

Dynamic Mechanical Analysis

The dynamic mechanical thermal properties of cured samples were obtained using a DMA 8000. Samples were tested in the single-cantilever mode at a frequency of 1 Hz and 0.2% strain. The relationship between storage modulus and tan δ versus temperature was determined with computerized heating from 30 to 250 °C at a heating rate of 2 °C min^{-1}. Rectangular bar specimens with dimensions of 50 × 5 × 2 mm^3 were used for this test.

Resin Fracture Toughness Test

The resin fracture toughness (K_{IC}) of the cured samples was examined according to the ASTM D5045-99, as described in our previously published paper.[14–16] A first crack at the notched tip of the sample was made using a fresh razor blade. The test was conducted at a speed of 10 mm min^{-1}, and the average values of K_{IC} from five tests were calculated. The K_{IC} was calculated using the following equation:

$$K_{IC} = \left(\frac{P_Q}{BW^{\frac{1}{2}}}\right) f(x), \tag{2}$$

where

$$f(x) = 6x^{\frac{1}{2}} \frac{[1.99 - x(1-x)(2.15 - 3.93x + 2.7x^2]}{(1+2x)(1-x)^{\frac{3}{2}}}.$$

Here, P_Q (kN), B (cm), W (cm), $f(x)$, and a represent the critical load for crack propagation, specimen thickness, specimen width, nondimensional shape factor, and crack length (cm), respectively. Additionally, $x = a/W$.

Tensile Testing

A tensile test was conducted according to ISO-527-1993 using an Instron 5582-100 kN machine at a speed of 10 mm min^{-1}. The specimen dimensions were 250 × 25 × 2.5 mm^3, and the gauge length was 50 ± 1 mm. The average values for five specimens were obtained.

Izod Notched Impact Strength Tests

The Izod notched impact strength was evaluated according to ISO 180 using a Tinius Olsen Model 92T Plastic Impact impact tester. The conditions for the test were 25 ± 2 °C and 60 ± 5% relative humidity. The average impact strength for at least five tested samples was obtained.

Morphology Analysis

SEM (JEOL JSM 6360, Tokyo, Japan) was used to observe a fracture surface, which was coated with gold.

RESULTS AND DISCUSSION

Epoxidation and Grafting Reaction Confirmation

The FTIR spectra of LO, uncured ELO, and CTBN-*g*-ELO were examined and compared to verify the success of both the epoxidation and the grafting reaction, as shown in Figure 2.

The main chemical groups of a triglyceride molecule, which characterized LO, were confirmed. The signals assigned to C═O and C—O stretching were observed via FTIR spectroscopy of LO at wave numbers of 1744 and 1160 cm^{-1}, respectively. The methylene groups were indicated by peaks at 2925, 2860, 1460, and 1380 cm^{-1}. The stretching vibrations of double bonds, that is, ═C—H, C═C, and cis CH═CH, were confirmed by the bands of 3010, 1650, and 720 cm^{-1},[37] respectively. Comparing the FTIR spectra of LO and ELO revealed that new signals corresponding to the oxirane ring appeared at 1240, 826, and 780 cm^{-1}. Additionally, the FTIR signal corresponding to the double bond at 3010 cm^{-1} disappeared for the ELO.

The synthesized ELO was mixed with CTBN to form grafted CTBN-*g*-ELO via a reaction between the oxirane group and carboxyl group. The FTIR spectra of CTBN-*g*-ELO exhibited a new peak at 3431 cm^{-1}, which is attributed to the hydroxy group in CTBN-*g*-ELO formed by the oxirane ring-opening reaction, compared with the spectra of ELO. Additionally, new peak appeared at 2236 cm^{-1}, which was assigned to the stretching vibration of C≡N in CTBN.[38] The transmittance signal at 826 cm^{-1}, corresponding to oxirane vibration with a reduced intensity, was retained after the grafting reaction. However, the peak at

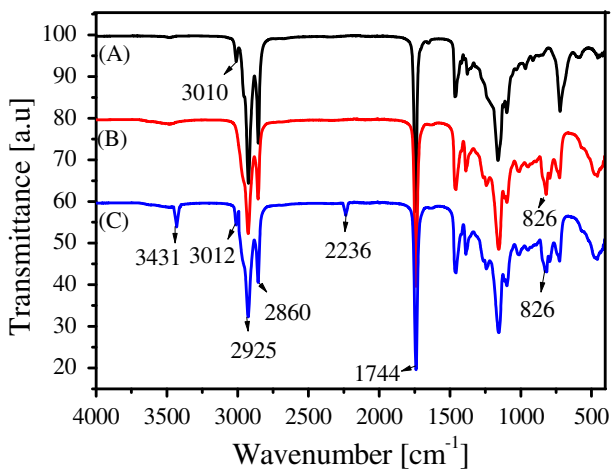

Figure 2. FTIR spectra of LO (a), ELO (b), and CTBN-*g*-ELO (c). [Color figure can be viewed at wileyonlinelibrary.com]

1744 cm^{-1} corresponding to the C═O stretching vibration was broadened, indicating the formation of an O═C—O ester bond due to the chemical reaction of CTBN with the ELO molecules. Furthermore, the peak at 3012 cm^{-1}, corresponding to the double bond, reappeared in the FTIR spectra of CTBN-*g*-ELO. The area of the peak corresponding to oxirane was used to calculate the grafting degree of CTBN-*g*-ELO.

^{1}H NMR was employed to confirm the success of the epoxidation and the grafting reaction. The ^{1}H NMR spectra of ELO (chloroform-*d*) exhibited a chemical shift at 2.9–3.1 ppm, corresponding to the epoxy groups, in agreement with the results of Park *et al.*[39] The ^{1}H NMR spectra of CTBN-*g*-ELO were examined to confirm the success of the grafting reaction. The chemical shifts at 1.25, 2.5–2.8, 5.3–5.7, and 2.9–3.1 ppm corresponded to (—CH_2—C—CN, —CH_2—C—C═C), (—C—CH—CN), (—CH═CH—, —CH═C), and oxirane groups, respectively. After the grafting reaction was complete, the grafting degree was determined to be 55.26% via a titration method.

The average molecular weight was used as another parameter to confirm the success of the grafting reaction. The average molecular weights of ELO and CTBN-*g*-ELO were examined via GPC, as shown in Table I.

The $\bar{M}_W$ and polydispersity index (PDI) were 1536 g mol^{-1} and 1.036, respectively, for ELO and 5600 g mol^{-1} and 1.056, respectively, for CTBN-*g*-ELO. These values indicate that after the grafting processing, the average molecular weight of CTBN-*g*-ELO was increased by a factor of approximately 3.6 compared with ELO. Additionally, the results suggest that the mole reaction ratio between the carboxyl group in CTBN and the epoxide group in ELO was approximately 1/1; that is, one carboxyl group helped to open one oxirane group, as the average molecular weight of CTBN was 3600 g mol^{-1}.

The synthesized CTBN-*g*-ELO was blended with EP by using a magnetic stirrer. FTIR spectroscopy was performed to confirm the reaction between the carboxyl group in CTBN-*g*-ELO and the oxirane group in the EP, as shown in Figure 3.

In Figure 3, both uncured EP and EP/15 CTBN-*g*-ELO exhibit peaks at 831 and 915 cm^{-1}, corresponding to the oxirane group. However, the intensities of the peaks at 831 and 915 cm^{-1} were reduced because the reaction between carboxyl and oxirane helped to open the oxirane ring. Additionally, the intensity of the peak corresponding to the hydroxyl group was increased for EP/15 CTBN-*g*-ELO. New peaks at 2236 and 3020 cm^{-1} corresponding to the C≡N and C═C groups, respectively, were observed in the FTIR spectra of the EP/15 CTBN-*g*-ELO mixture. The molecular weight of EP and the EP/15 CTBN-*g*-ELO mixture was determined to confirm the reaction between CTBN-*g*-ELO and EP, as shown in Table I. The average molecular weight of EP/15 CTBN-*g*-ELO was 1682 g mol^{-1}, and the PDI was 1.26. The low PDI indicated that the molecular weight was distributed in a narrow range. This result confirms the reaction between the carboxyl group in CTBN-*g*-ELO and the oxirane group in the EP.

Rheological Testing

The rheological properties, particularly viscosity of uncured resin, significantly affect the final properties of composite material. These parameters are related to the penetration ability of resin

Table I. Average Molecular Weight ($\bar{M}_W$) and PDI of ELO, CTBN-*g*-ELO, EP, and the EP/15 CTBN-*g*-ELO Mixture According to GPC

	ELO	CTBN-*g*-ELO	EP	15 CTBN-*g*-ELO/EP
$\bar{M}_{W\,(g\,mol^{-1})}$	1536	5600	780	1682
PDI	1.036	1.052	1.18	1.26

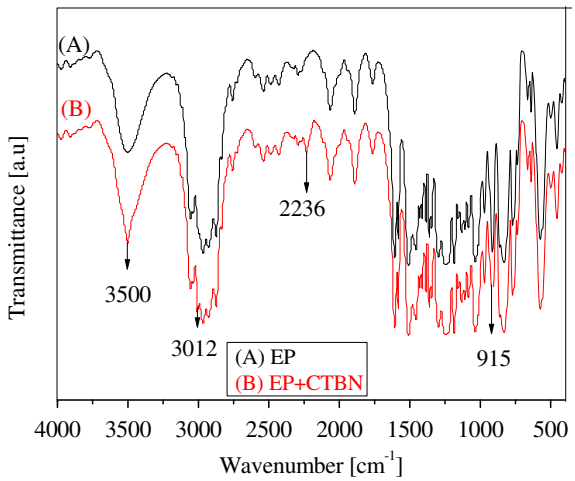

Figure 3. FTIR spectra of uncured EP (a) and a mixture of EP with 15 wt % CTBN-*g*-ELO. [Color figure can be viewed at wileyonlinelibrary.com]

into reinforcement material. In general, a fluid can be classified into two types—Newtonian or non-Newtonian according to its rheological properties. The rheological properties of uncured EP resin with and without CTBN-*g*-ELO are presented in Figure 4.

The pristine uncured EP and 5 phr CTBN-*g*-ELO-filled EP exhibited Newtonian behavior because viscosity was not dependent on shear rate. At a higher CTBN-*g*-ELO content, EP exhibited non-Newtonian behavior, with a shear-thinning characteristic. In this case, viscosity decreased as shear rate increased up to 250 s^{-1}, due to the significant increase in the CTBN-*g*-ELO agglomerates. These agglomerates hindered the alignment of the EP chains. With an increase in the shear rate, the agglomerates decomposed, and EP chains aligned rapidly in the direction of increasing shear rate, resulting in shear-thinning behavior. At a shear rate of >250 s^{-1}, the viscosity was constant. The results in Figure 4 also indicate that shear stress and shear rate had a simple linear relationship for all CTBN-*g*-ELO contents. Both the shear stress and viscosity increased with CTBN-*g*-ELO content.

Mechanical Properties of CTBN-*g*-ELO-Filled EP

The typical stress–strain relationship of the cured EP with various CTBN-*g*-ELO contents was plotted, as shown in Figure 5.

With the increasing CTBN-*g*-ELO content, the slopes of curves in Figure 5 decreased, while the strain increased. The maximum stress increased with the CTBN-*g*-ELO content, and the optimum value was observed at 15 phr. The presence of CTBN-*g*-ELO reduced the crosslinking density and enhanced the main-chain

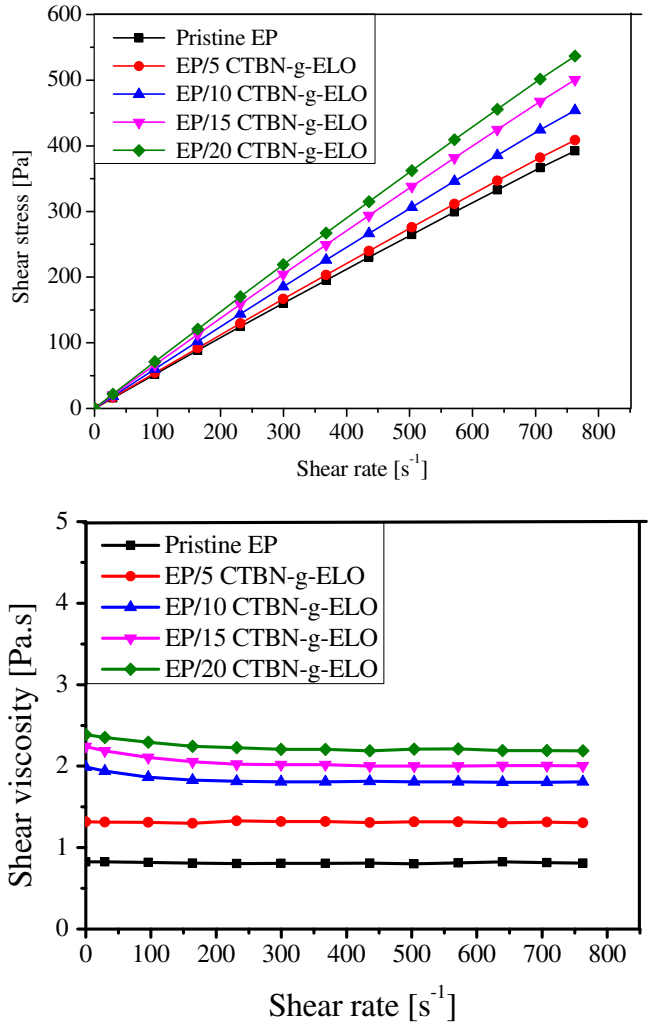

Figure 4. Rheological properties of EP with different contents of CTBN-*g*-ELO. [Color figure can be viewed at wileyonlinelibrary.com]

mobility because of the increased ductility and strain. Additionally, the higher tensile strength results from higher crystallinity due to the chains align and for the crystalline phase during the tensile test.

The effects of the CTBN-*g*-ELO on the load–displacement curves, impact strength, and K_{IC} were examined, as shown in Figure 6 and Table II.

The load–displacement curves exhibited a linear relationship until complete fracture, as shown in Figure 6. Thus, the maximum force was used to calculate the K_{IC} values of cured EP. The results in Table II indicate that CTBN-*g*-ELO significantly affected both impact strength and K_{IC} values of EP. The impact strength and K_{IC} increased with CTBN-*g*-ELO content, and optimal values were obtained with 15 phr CTBN-*g*-ELO. With the addition of 15 phr CTBN-*g*-ELO, the impact strength and K_{IC} of EP increased by 91.82 and 67.69%, respectively. This may be because the CTBN-*g*-ELO absorbed external force or altered the direction of crack growth, enhancing the impact strength and toughness. Additionally, the reaction of carboxyl group in CTBN-*g*-ELO with oxirane group extended molecular chain of

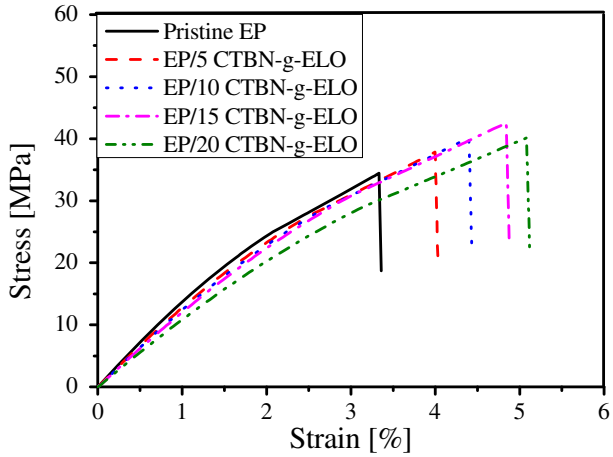

Figure 5. Typical true stress–strain curves obtained via tensile testing of EP with various contents of CTBN-*g*-ELO. [Color figure can be viewed at wileyonlinelibrary.com]

EP. This reaction was confirmed by comparing the FTIR spectra of uncured EP and uncured EP/CTBN-*g*-ELO, as shown in Figure 3. When the CTBN-*g*-ELO content was >15 phr, both impact strength and K_{IC} decreased because of the size effect of CTBN-*g*-ELO particles located in epoxy matrix. The maximum improvements (percent) of the K_{IC} and tensile strength of EP achieved using CTBN-*g*-ELO in this study and using other additives in previous studies are compared in Table III.

The data in Table III indicate that the maximum improvement (percent) of K_{IC} value of EP achieved using CTBN-*g*-ELO was only 67.69%, which is smaller than those achieved using CTBN and ECO and larger than that in the case of a silanized micro/-nanosized white bamboo fibrils (s-MWBF)-filled EP. However, the improvement of tensile strength of EP with addition of CTBN-*g*-ELO was 23.61%, which is larger than those achieved with addition of CTBN and s-MWBF. Additionally, the use of CTBN reduced tensile strength by approximately 12.35%. The

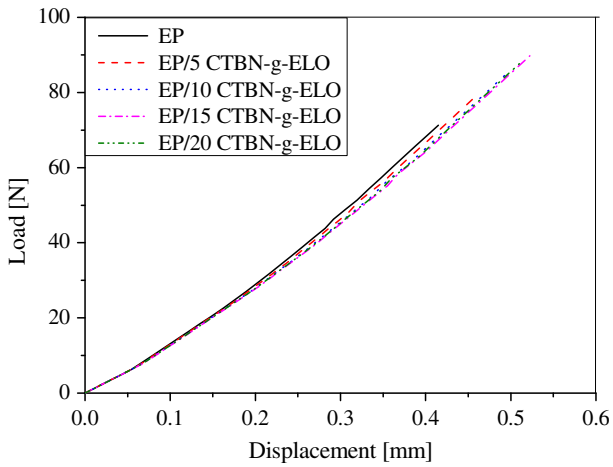

Figure 6. Typical load–displacement curves obtained via resin fracture toughness testing of cured EP with and without CTBN-*g*-ELO. [Color figure can be viewed at wileyonlinelibrary.com]

Table II. Effect of the CTBN-*g*-ELO Content on the Mechanical Characteristics of DER331 EP

CTBN-*g*-ELO contents (phr)	Izod impact strength (kJ m^{-2})	K_{IC} (MPa $m^{-1/2}$)
0	6.1 ± 0.16	0.65 ± 0.05
5	9.0 ± 0.28	0.72 ± 0.08
10	10.8 ± 0.39	0.87 ± 0.03
15	11.7 ± 0.26	1.09 ± 0.06
20	9.6 ± 0.42	0.89 ± 0.09

improvements of mechanical properties and fracture toughness achieved using additives depended on the type of additive, type of resin, and testing conditions. The CTBN-*g*-ELO, which had a larger molecular weight than both pristine CTBN and ELO, improved the fracture toughness and mechanical properties. Furthermore, the CN, OH, and COOH groups formed strong connections between CTBN-*g*-ELO and EP via hydrogen bonds, for example, opening the oxirane group, compared with the pristine CTBN and ELO.

The fracture surface of the EP was examined in detail to confirm the foregoing mechanical properties.

The results in Figure 7(a) indicate that the pristine EP had a smooth and glassy fractured surface, which is characteristic of brittle material. In contrast, the EP filled with 15 phr CTBN-*g*-ELO had a rougher and tougher surface with spherical particles. The appearance of spherical particles of CTBN-*g*-ELO indicated the existence of a two-phase system after curing. As shown in Figure 7(b), the cracks appeared to stop or change their growth direction, as indicated by yellow arrows, at the CTBN-*g*-ELO particles. At high CTBN-*g*-ELO contents, the agglomeration phenomenon was observed. The agglomerated particles, as shown in Figure 7(c), were considered as the reason for the reductions in the impact strength and K_{IC}.

Thermal Stability

TGA–differential thermogravimetry (DTG) was used to evaluate thermal stabilities of the CTBN-*g*-ELO, cured pristine epoxy, and cured CTBN-*g*-ELO-modified EP under nitrogen, as shown in Figure 8.

The CTBN-*g*-ELO exhibited one-step thermal decomposition, with maximum degradation at 356.56 °C owing to the thermolysis of the main chain. In contrast, a two-step thermal-degradation process was observed for the cured epoxy with and without CTBN-*g*-ELO. The first decomposition process occurred around 370 °C, implying that samples had same thermal-decomposition pathway. This pathway was probably induced by dehydrogenation and aromatization of alkyl at this temperature, along with decomposition of CTBN-*g*-ELO. The second decomposition step occurred around 570 °C and is attributed to the further degradation of char layer. Compared with the neat epoxy, the maximum degradation temperature was shifted to lower values with the presence of CTBN-*g*-ELO. The maximum degradation temperature of the pristine EP was 546.98 and 376.62 °C.

Table III. Comparison of the Fracture Toughness and Mechanical Properties of EP with Various Additives

Additives	Maximum change in K_{IC} (%)	Maximum change in tensile strength (%)	Maximum change in T_g (%)	Ref.
CTBN	77.62	−12.35	−39.51	34
ECO	105.99	No data	−33.58	29
CTBN-*g*-ELO	67.69	23.61	−8.56	This work
s-MWBF	25.39	7.21	7.31	16

ECO, epoxidized castor oil; s-MWBF, silanized micro/nanosized white bamboo fibrils.

The maximum degradation temperature of EP/CTBN-*g*-ELO was 531.69 and 361.83°C. Additionally, the CTBN-*g*-ELO-modified EP exhibited a lower onset temperature for initial degradation (T_i). The initial degradation of pristine epoxy occurred at 322.8 °C, whereas that of the 15 phr CTBN-*g*-ELO-modified EP occurred at 309.6 °C. The reduction in the T_i of EP with the presence of CTBN-*g*-ELO was due to the degradation of CTBN-*g*-ELO, along with the reduction in crosslinking density.

Thermomechanical Properties (DMTA) and DSC of CTBN-*g*-ELO-Filled EP

The effect of the CTBN-*g*-ELO loading on the T_g of EPs was investigated using DSC and DMTA.

The results in Figure 9 indicate that the T_g of EP shifted to a lower temperature range with the presence of CTBN-*g*-ELO because of the effect of CTBN-*g*-ELO on the molecular mobility of epoxy chain. The presence of CTBN-*g*-ELO reduced the crosslinking density and enhanced the molecular mobility of epoxy chain. The T_g values of EP with the addition of 0, 5, 10, 15, and 20 phr CTBN-*g*-ELO were 174.5, 166.8, 158.9, 154.5, and 151.9 °C, respectively.

The dynamic mechanical thermal properties of the EP with different CTBN-*g*-ELO contents are shown in Figure 10.

The parameter from the DMTA test was used to determine the crosslinking density, which is one of important factors related to thermal stability of epoxy. The crosslinking density of the EP with and without CTBN-*g*-ELO was calculated as follows.[40]

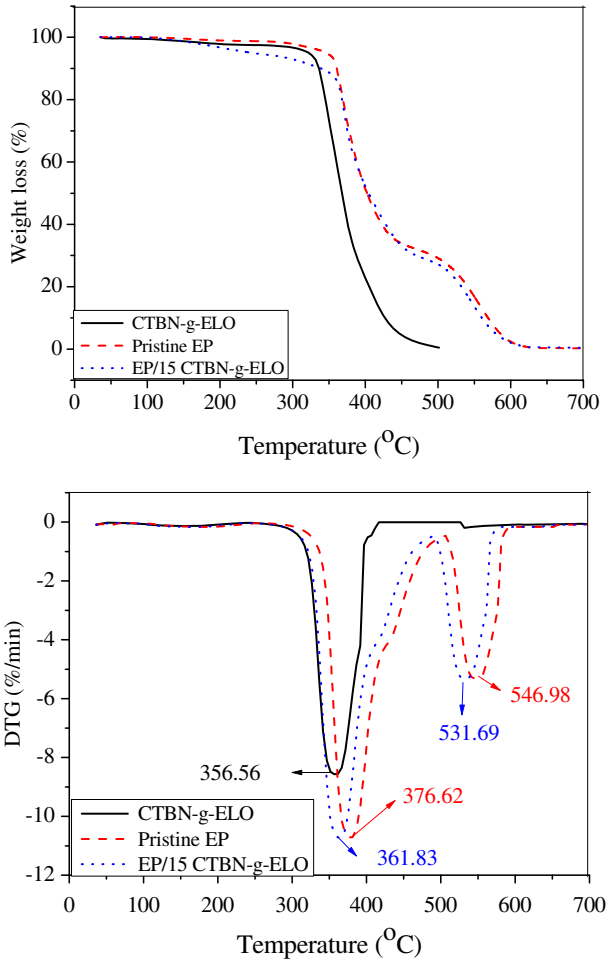

Figure 8. TGA–DTG results for CTBN-*g*-ELO, pristine EP, and modified epoxy. [Color figure can be viewed at wileyonlinelibrary.com]

$$\rho = \frac{G'}{RT} \quad (3)$$

Here, ρ represents the crosslinking density (mol cm^{-3}), G' represents the storage modulus of the sample in the rubbery region (J cm^{-3}), R represents the gas constant (8.314412 J K^{-1} mol^{-1}), and T (K) represents the absolute temperature at which G' is determined. $T = T_g + 50$ °C + 273 (K).[41] The crosslinking densities of the EP with 0, 5, 10, 15, and 20 phr CTBN-*g*-ELO were 7.39×10^9, 6.78×10^9, 6.58×10^9, 6.43×10^9, and 6.23×10^9 mol cm^{-3}, respectively. These

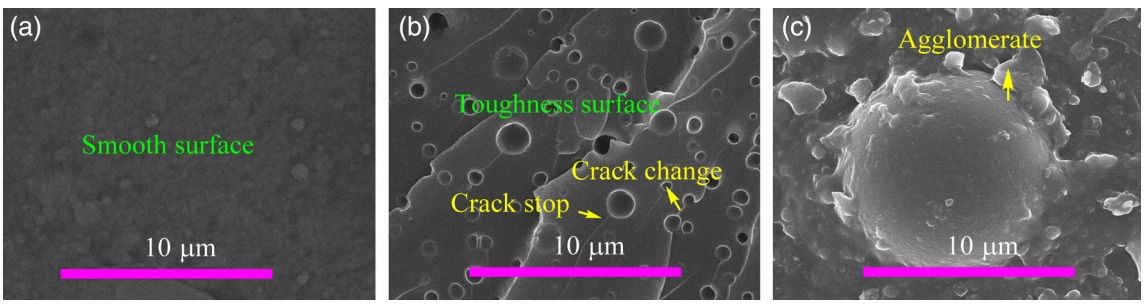

Figure 7. SEM images showing the facture surfaces of cured pristine EP (a), cured EP/15 CTBN-*g*-ELO (b), and cured EP/20 CTBN-*g*-ELO (c). [Color figure can be viewed at wileyonlinelibrary.com]

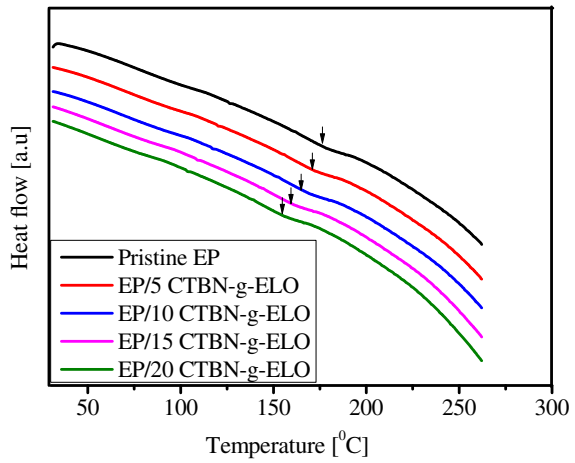

Figure 9. DSC curves of epoxy with various contents of CTBN-*g*-ELO. [Color figure can be viewed at wileyonlinelibrary.com]

results indicate that the crosslinking density decreased with the increasing CTBN-*g*-ELO content, which contributed to the foregoing results for the thermal stability.

The storage moduli of EP decreased with increasing CTBN-*g*-ELO content as shown in Figure 10, due to the reduction in

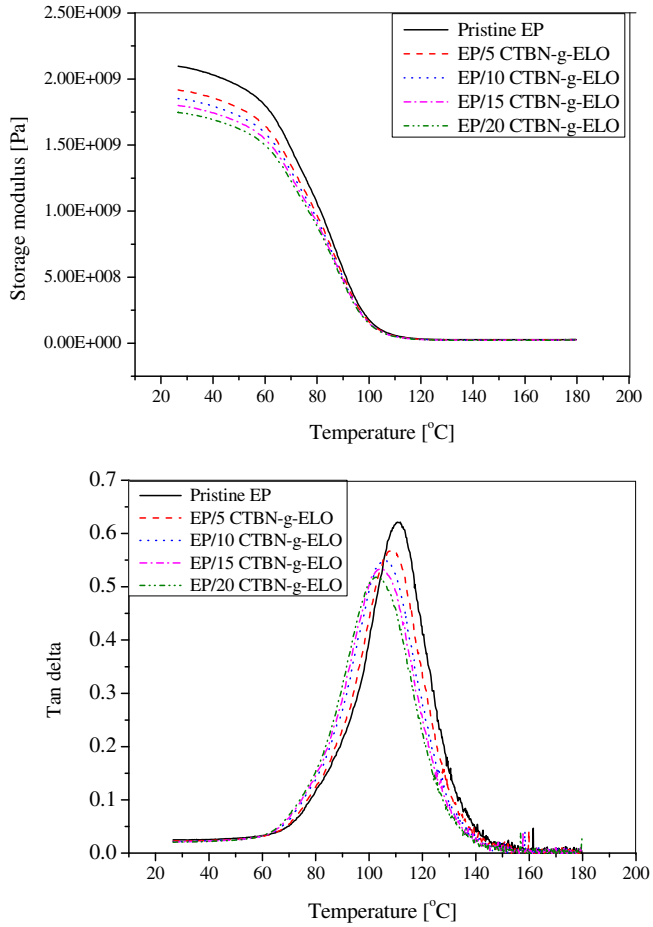

Figure 10. Storage modulus and tan δ versus the temperature of EP with different CTBN-*g*-ELO contents. [Color figure can be viewed at wileyonlinelibrary.com]

crosslinking density of EP. The same trend was observed for the tan σ value. The maximum tan σ values for the CTBN-*g*-ELO-modified epoxy samples were lower than those of the pristine epoxy. Additionally, the presence of CTBN-*g*-ELO reduced the T_g of EP. The T_g values of the EP with 0, 5, 10, 15, and 20 phr CTBN-*g*-ELO were 112.1, 108.3, 105.8, 104.3, and 102.5 °C, respectively. The decreased T_g is ascribed to the plasticization of CTBN-*g*-ELO on the epoxy matrix and the low T_g of rubber. In addition, the T_g was closely related to the crosslinking density.[37] A reduction in the crosslinking density decreased the T_g. A comparison of the maximum change in T_g in the present study with the results of previous studies is presented in Table III. The data indicate that with the addition of CTBN, the ECO, and CTBN-*g*-ELO exhibited decreasing T_g values. In contrast, the addition of s-MWBF increased the T_g owing to the higher crosslinking density.

CONCLUSIONS

A novel method was developed for the synthesis of CTBN-*g*-ELO from CTBN and ELO, and the CTBN-*g*-ELO was used as a toughener for EP. The ELO was successfully fabricated from LO via epoxidation processing. The effects of the CTBN-*g*-ELO content on physicomechanical properties of EP were investigated in detail. With the presence of CTBN-*g*-ELO, the tensile strength, impact strength, and fracture toughness of the EP increased (up to 15 phr CTBN-*g*-ELO) because of the cavitation/debonding of CTBN-*g*-ELO from epoxy matrix. Compared with previously reported additives, the CTBN-*g*-ELO improved both the mechanical properties and fracture toughness of EP.

ACKNOWLEDGMENT

This research was funded by the Vietnam National Foundation for Science and Technology Development (NAFOSTED) under grant number 104.02-2017.15.

REFERENCES

1. Cui, J.; Xie, A.; Zhou, S.; Liu, S.; Wang, Q.; Wu, Y.; Meng, M.; Lang, J.; Zhou, Z.; Yan, Y. *J. Colloid Interface Sci.* **2019**, *533*, 278.
2. Zhao, W.; Lee, J.; Kim, H.; Jang, H.; Nam, J.; Kim, K.; Suhr, J. *Polym. Test.* **2019**, *74*, 99.
3. Astashkin, V.; Shmatkov, S.; Shmatkov, A. *Proc. Eng.* **2016**, *150*, 1701.
4. Sun, M.; Dai, B.; Liu, K.; Yao, K.; Zhao, J.; Lyu, Z.; Wang, P.; Ding, Y.; Yang, L.; Han, J.; Zhu, J. *Compos. Sci. Technol.* **2018**, *164*, 129.
5. Hoang, S. L.; Vu, C. M.; Pham, L. T.; Choi, H. J. *Polym. Bull.* **2018**, *75*, 2607.
6. Vu, C. M.; Choi, H. J. *Polym. Plast. Technol. Eng.* **2016**, *55*, 1048.
7. Cheng, X.; Wu, Q.; Morgan, S. E.; Wiggins, J. S. *J. Appl. Sci.* **2017**, *134*, 44775.
8. Vu, C. M.; Nguyen, D. D.; Sinh, L. H.; Pham, T. D.; Pham, L. T.; Choi, H. J. *Polym. Test.* **2017**, *61*, 150.

9. Vu, C. M.; Sinh, L. H.; Nguyen, D. D.; Thi, H. V.; Choi, H. J. *Polym. Test.* **2018**, *71*, 200.
10. Zhao, X.; Li, Y.; Chen, W.; Li, S.; Zhao, Y.; Du, S. *Compos. Sci. Technol.* **2019**, *171*, 180.
11. Lei, F.; Zhang, C.; Cai, Z.; Yang, J.; Sun, H.; Sun, D. *Polymer*. **2018**, *150*, 44.
12. Cha, J.; Jun, G. H.; Park, J. K.; Kim, J. C.; Ryu, H. J.; Hong, S. H. *Compos. B: Eng.* **2017**, *129*, 169.
13. Ma, C.; Liu, H. Y.; Du, X.; Mach, L.; Xu, F.; Mai, Y. W. *Compos. Sci. Technol.* **2015**, *114*, 126.
14. Vu, C. M.; Nguyen, L. T.; Nguyen, T. V.; Choi, H. J. *Polym. Korea*. **2014**, *38*, 726.
15. Pham, T. D.; Vu, C. M.; Choi, H. *J. Polym. Sci. Ser. A*. **2017**, *59*, 437.
16. Vu, C. M.; Sinh, L. H.; Choi, H. J.; Pham, T. D. *Cellulose*. **2017**, *24*, 5475.
17. Ladani, R. B.; Bhasin, M.; Wu, S.; Ravindran, A. R.; Ghorbani, K.; Zhang, J.; Kinloch, A. J.; Mouritz, A. P.; Wang, C. H. *Eng. Fract. Mech.* **2018**, *203*, 102.
18. Klingler, A.; Bajpai, A.; Wetzel, B. *Eng. Fract. Mech.* **2018**, *203*, 81.
19. Ekrem, M.; Avcı, A. *Compos. B: Eng.* **2018**, *138*, 256.
20. Eskizeybek, V.; Yar, A.; Avcı, A. *Compos. Sci. Technol.* **2018**, *157*, 30.
21. Eskizeybek, V.; Avci, A.; Gülce, A. *Compos. Part A: Appl. Sci. Manuf.* **2014**, *63*, 94.
22. Vu, C. M.; Nguyen, D. D.; Sinh, L. H.; Choi, H. J.; Pham, T. D. *Macromol. Res.* **2018**, *26*, 54.
23. Guan, F.; Chen, S.; Yao, J.; Zheng, W.; Wang, H. *J. Mater. Sci. Technol.* **2016**, *32*, 153.
24. Faria, M.; Vilela, C.; Silvestre, A. J. D.; Deepa, B.; Resnik, M.; Freire, C. S. R.; Cordeiro, N. *Carbohydr. Polym.* **2019**, *206*, 86.
25. Yuan, H.; Shi, H.; Qiu, X.; Chen, Y. *J. Biomater. Sci. Polym. Ed.* **2016**, *27*, 263.
26. Vu, C. M.; Nguyen, D. D.; Sinh, L. H.; Choi, H. J.; Pham, T. D. *Polym. Bull.* **2018**, *75*, 4769.
27. Gupta, A. P.; Ahmad, S.; Dev, A. *Polym. Eng. Sci.* **2011**, *51*, 1087.
28. Jin, F. L.; Park, S. J. *Polym. Int.* **2008**, *57*, 577.
29. Park, S. J.; Jin, F. L.; Lee, J. R. *Macromol. Chem. Phys.* **2004**, *205*, 2048.
30. Paluvai, N. R.; Mohanty, S.; Naya, S. K. *Polym. Adv. Technol.* **2015**, *26*, 1575.
31. Niedermann, P.; Szebényi, G.; Toldy, A. *J. Polym. Environ.* **2014**, *22*, 525.
32. Sarwono, A.; Man, Z.; Bustam, M. A. *J. Polym. Environ.* **2012**, *20*, 540.
33. Zhu, L.; Jin, F. L.; Park, S. J. *Bull. Korean Chem. Soc.* **2012**, *33*, 2513.
34. Wang, L.; Tan, Y.; Wang, H.; Gao, L.; Xiao, C. *Chem. Phys. Lett.* **2018**, *699*, 14.
35. Wang, F.; Drzal, L. T.; Qin, Y.; Huang, Z. *Compos. Part A: Appl. Sci. Manuf.* **2016**, *87*, 10.
36. Zhang, J.; Deng, S.; Wang, Y.; Ye, L. *Compos. Part A: Appl. Sci. Manuf.* **2016**, *80*, 82.
37. Yim, Y. J.; Rhee, K. Y.; Park, S. J. *Compos. Part B*. **2017**, *131*, 144.
38. Konnola, R.; Joji, J.; Parameswaranpillai, J.; Joseph, K. *RSC Adv.* **2015**, *5*, 61775.
39. Park, S. J.; Jin, F. L.; Lee, J. R. *Mater. Sci. Eng. A*. **2004**, *374*, 109.
40. Yu, J. W.; Jung, J.; Choi, Y. M.; Choi, J. H.; Yu, J.; Lee, J. K.; You, N. H.; Goh, M. *Polym. Chem.* **2016**, *7*, 36.
41. Xin, J.; Zhang, P.; Huang, K.; Zhang, J. *RSC. Adv.* **2014**, *4*, 8525.